3

A summary of the *Galileo* mission and its observations of Io

Jason Perry, Rosaly M. C. Lopes, John R. Spencer, and Claudia Alexander

3.1 *GALILEO* ERA: 1995–2003

Even before the arrival of the two *Voyager* spacecraft at Jupiter in 1979, planning began at the Jet Propulsion Laboratory (JPL) for the Jupiter Orbiter with Probe. The mission received Congressional approval in 1977 and was renamed *Galileo* in 1978. The launch of *Galileo*, originally planned for 1982, was repeatedly delayed through the 1980s, first due to development problems with the Space Shuttle, then due to issues with the upper stage motor, and finally due to the Space Shuttle *Challenger* disaster. With a firm political commitment to launch *Galileo* from the Space Shuttle, the launch would have to wait until 18 October 1989. Due to safety recommendations following the *Challenger* disaster, *Galileo* was forced to use a lower powered upper stage than originally planned, requiring it to spiral out to Jupiter, using gravity assists at Venus and Earth to boost it on its way (Harland, 2000).

As one of NASA's unmanned Flagship-class missions, *Galileo* was heavily instrumented, with five remote-sensing instruments and six fields and particles instruments (Table 3.1), plus celestial mechanics and radio propagation experiments. The five imaging instruments covered a wide range of wavelengths, from the extreme ultraviolet to the mid-infrared. Among the objectives for the remote-sensing instruments were characterization of Io's surface morphology, geology, and physical state; investigation of the surface mineralogy and distribution of compositional units; investigation of the extent and characteristics of volcanic activity, and studies of the atmosphere and its relation to volcanic plumes.

The imaging system on *Galileo*, known as the solid-state imaging system (SSI), was comprised of a charge-coupled device with an 800 × 800-pixel array on a narrow-angle Cassegrain telescope (Belton *et al.*, 1992). The SSI camera had eight filter positions ranging from a violet filter centered at 418 nm to a 1MC filter with a bandpass centered at 990 nm (McEwen *et al.*, 1998a). The near-infrared mapping spectrometer (NIMS) instrument was a scanning instrument capable of taking a

Table 3.1. *Galileo* science instrument payload.

Device	Institution	Principal investigator	Primary measurements
Atmosphere structure instrument (ASI)	Ames Research Center	A. Seiff	Pressure, temperature, and density
Nephelometer (NEP)	Ames Research Center	B. Ragent	Cloud particle size, shape, and number density
Helium abundance detector (HAD)	University of Bonn	Ulf von Zahn	He/H_2 ratio to ~0.1%
Net flux radiometer (NFR)	Ames Research Center	R. Boese	Net planetary and solar fluxes, cloud locations, water and ammonia abundance
Neutral mass spectrometer (NMS)	Goddard Space Flight Center	H. Niemann	Composition in 1–150 AMU range
Lightning and radio emissions detector (LRD)	Bell Laboratories Max-Planck Institute	L. Lanzerotti K. Rinnert	Existence and characteristics of lightning
Energetic particle instrument (EPI)	University of Kiel, Ames Research Center	H. Fischer J. Mihalov	Energetic particle distribution from 5 Jupiter radii to entry
Solid-state imaging (SSI)	National Optical Astronomy Observatories	M. Belton	Map Galilean satellites at roughly 1-km resolution, and monitor atmospheric circulation
Near-infrared mapping spectrometer (NIMS)	JPL	R. Carlson	Surface composition, atmospheric composition and temperature
Ultraviolet spectrometer (UVS)	University of Colorado	C. Hord I. Stewart	Gases and aerosols in Jovian atmosphere, auroral emissions, satellite atmospheric airglow
Extreme-ultraviolet spectrometer (EUV)	University of Colorado	C. Hord K. Simmons	S, O ion emissions of the Io torus, and atomic and molecular H auroral and airglow emissions
Photopolarimeter and radiometer (PPR)	Goddard Institute for Space Studies	J. Hansen	Distribution and character of atmospheric particles; surface temperatures of the satellites
Magnetometer (MAG)	University of California	M. Kivelson	Monitor magnetic field for strength and changes
Energetic particles detector (EPD)	Johns Hopkins Applied Physics Laboratory	D. Williams	High-energy electrons, protons, and heavy ions in the magnetosphere and processes affecting these populations
Plasma detector subsystem (PLS)	University of Iowa	L. Frank	Composition, energy, and 3-D distribution of low- to medium-energy electrons and ions
Plasma wave subsystem (PWS)	University of Iowa	D. Gurnett	Electromagnetic waves and wave–particle interactions
Dust detector subsystem (DDS)	Max Planck Institut für Kernphysik	E. Grun H. Krueger	Mass, velocity, and charge of dust particles
Heavy ion counter (HIC)	California Institute of Technology	T. Garrard E. Stone	Composition, and energy of low-energy ions in the environment
Celestial mechanics	JPL	J. Anderson	Masses and internal structures of Jupiter and its satellites
Radio propagation	Stanford University	H. T. Howard	Atmospheric structure and objects' radii

408-wavelength spectrum in the range 0.7–5.2 μm, therefore measuring both reflected sunlight and thermal emission (Carlson *et al.*, 1992). NIMS formed spectra using 17 detectors in combination with a moving grating. The 17 wavelengths (spaced across the wavelength range) obtained for each grating position were acquired simultaneously. During the *Galileo* nominal mission, and the *Galileo* Europa mission (GEM), two of the NIMS detectors stopped working, and the sensitivity of the first two detectors was considerably reduced. Prior to the first NIMS observations in the Io fly-by I24, grating motion ceased, probably from radiation damage to the electronics. Therefore, the observations during the Io fly-bys obtained only 13 wavelengths (though acquiring 24 samples of eacb instead of 1), in the rage 1.0–4.7 μm. The reduced number of wavelengths was suitable for temperature determination and band ratio mapping (for SO_2) but the instrument's ability to search for unknown surface compounds was compromised.

The photopolarimeter and radiometer (PPR) instrument (Russell *et al.*, 1992) conducted three separate types of measurements in one instrument: photometry, polarimetry, and radiometry. The radiometry experiment was most useful for Io, measuring thermal emission at much longer wavelengths (visible–100 μm), and thus detecting colder temperatures than NIMS. This allows for more effective estimation of the total heat flow from Io's interior as well as measurements of the thermal emission from the sunlit surface. PPR's low spatial resolution limited its usefulness for Io studies until the close fly-bys in 1999 and onward. In addition *Galileo's* ultraviolet spectrometer (UVS) obtained spectra of Io in the 2,100–3,200-Å region, though radiation noise near Jupiter did not permit useful observations from ranges less than about 500,000 km.

The six *in situ* instruments (Russell *et al.*, 1992; see Table 3.1) consisted of a magnetometer (MAG), an energetic particles detector (EPD), a plasma detector subsystem (PLS), a plasma wave subsystem (PWS), a dust detector subsystem (DDS), and a heavy ion counter (HIC). The MAG monitored magnetic fields of the environment for overall strength and the smaller changes related to the dynamics of the system such as the presence of large-scale waves. The particle energy spectrum in its totality was covered by three instruments: an EPD, which measured the energetic end of the particle energy range, from 20–890 keV – exact range being dependent upon the MeV per nucleon measured; a PLS, which measured the medium- to low-energy range of the particle spectrum, from 1 eV to 50 keV; and an HIC, which measured energetic heavy particles from 6–200 MeV per nucleon. These instruments gathered information on the velocity and density of the plasma, and also served as mass spectrometers. The EPD measured, among other things, elemental species of Helium through Iron from 10 keV per nucleon to 15 MeV per nucleon, the PLS measured masses largely in a range from 1–18 atomic mass units (AMU), and the HIC measured typically 6–18 MeV per nucleon: oxygen, sodium, carbon, sulfur, etc. The PWS acted as a radio receiver, picking up electric and magnetic signals in the range 5 Hz to 5 MHz on the electric antenna, and 5 Hz to 160 kHz on the magnetic antenna. The DDS detected the impacts of mass 10^{-19} to 10^{-9} kg. The PWS detected plasma waves and other radio signals in the environment such as the characteristic signal of plasma losing energy while gyrating around field lines (gyrofrequencies), the

characteristic signal of large-scale oscillations of the plasma in the field (plasma frequencies), and other characteristic motions of plasma. The fields and particles instruments worked together to investigate the environment of Io with more synergy than common with remote-sensing instruments. This was because magnetic field measurements as well as particle density measurements were required to properly determine selected characteristic parameters of the plasma activity, not only at Io but throughout the magnetosphere. The investigation of Io's interaction with Jupiter's magnetosphere was one of the major objectives of the *Galileo* mission. Among the questions these fields and particles instruments aimed to answer were: Did Io generate its own magnetic field? How significant was Io's influence on the magnetosphere of Jupiter?

The mission plan for *Galileo* called for 11 orbits of Jupiter following orbit insertion on 7 December 1995. During each orbit except the 5th, when *Galileo* and Jupiter were in solar conjunction, *Galileo* would fly-by one of the Galilean satellites: 4 fly-bys of Ganymede, 3 fly-bys of Callisto, and 3 fly-bys of Europa (Table 3.2). *Galileo*'s only close approach of Io would take place shortly before orbit insertion, otherwise it would stay well outside the orbit of Io to prevent encountering dangerous radiation. During the mission, thousands of images of Io were expected, including a number of movies showing variability within Io's volcanic plumes. Unfortunately, *Galileo*'s high-gain antenna failed to deploy. The antenna was designed to fold up like an umbrella to allow the spacecraft to be stowed in the Space Shuttle's cargo bay, and then unfurl during cruise to Jupiter. However, during deployment, one of the pins that made up the structural framework of the antenna became stuck. Due to this malfunction, the low-gain antenna (LGA) would have to be used for the duration of the mission, dramatically reducing the size of the data set returned by *Galileo*. Instead of returning data at an impressive rate of 134 kilobits per second with the high-gain antenna, *Galileo* was expected to achieve only 10 bits per second with the LGA. Thankfully, improved compression algorithms and data management on the spacecraft and upgrades to the Deep Space Network on Earth allowed the effective information flow from *Galileo* through the LGA to increase by a factor of 100. While, this still meant that the data set from *Galileo* of Io would be much smaller than expected (preventing the much-anticipated plume movies), the bandwidth was adequate for most science objectives to be accomplished.

3.2 JOI AND "THE LOST IO FLY-BY"

The only Io fly-by during the nominal *Galileo* mission took place shortly before Jupiter orbit insertion (JOI). The fly-by occurred at an altitude of 897 km over 8.5° south latitude, 101.1° west longitude (Anderson *et al.*, 1996). This in-bound fly-by would allow for remote-sensing observations of the anti-Jovian hemisphere, as well as investigations of Io's possible magnetic field and interactions between Io and Jupiter's magnetic field. Then, with just 2 months to go until arrival at Jupiter, the planned

Table 3.2. *Galileo* orbits and Io activities.

Orbit	Fly-by satellite	Date of main fly-by in orbit	Closest approach distance to Io (km)	Notable Io activities
J0	Io	12/7/1995	897	Close fly-by: fields and particles observations, no remote sensing. Gravitational detection of Io's core
G1	Ganymede	6/27/1996	697,000	Distant observations of surface changes since *Voyager*, NIMS dayside and nightside maps, high-phase imaging, first eclipse images
G2	Ganymede	9/6/1996	441,000	Color imaging of anti-Jupiter hemisphere, NIMS maps
C3	Callisto	11/4/1996	244,000	Topography of anti-Jupiter hemisphere, high-phase imaging of the sodium cloud
E4	Europa	12/19/1996	321,000	Global color imaging
5	None			
E6	Europa	2/20/1997	401,000	Eclipse imaging
G7	Ganymede	4/5/1997	531,000	NIMS observations of Loki
G8	Ganymede	5/7/1997	956,000	Eclipse imaging, auroral emissions
C9	Callisto	6/25/1997	607,000	Discovery of Pillan eruption
C10	Callisto	9/17/1997	319,000	Dark Pillan deposits first seen
E11	Europa	11/6/1997	780,000	SSI plume inventory
E12	Europa	12/16/1997	485,000	NIMS spectral maps
13	None		438,000	
E14	Europa	3/29/1998	252,000	Multi-spectral color of anti-Jupiter hemisphere
E15	Europa	5/31/1998	312,000	Best UVS observation, color eclipse imaging
E16	Europa	7/21/1998	702,000	NIMS spectral maps
E17	Europa	9/26/1998	800,000	
E18	Europa	11/22/1998	996,000	
E19	Europa	2/1/1999	856,000	
C20	Callisto	5/5/1999	789,000	NIMS spectral maps
C21	Callisto	6/30/1999	127,000	Best SSI resolution yet on the anti-Jupiter hemisphere
C22	Callisto	8/14/1999	737,000	Distant plume monitoring, NIMS maps
C23	Callisto	9/16/1999	448,000	
I24	Io	10/11/1999	611	First close-up remote sensing
I25	Io	11/26/1999	301	Tvashtar eruption images (SSI, NIMS)
E26	Europa	1/03/2000	340,000	Color imaging of Loki–Daedaldus region, NIMS maps
I27	Io	2/22/2000	198	Trouble-free fly-by, high-resolution remote sensing
G28	Ganymede	5/20/2000	379,000	
G29	Ganymede	12/28/2000	963,000	Distant imaging: Tvashtar plume, NIMS maps
C30	Callisto	5/25/2001	342,000	NIMS dayside, nightside maps
I31	Io	8/6/2001	194	Discovery of Thor eruption (NIMS and SSI), high-resolution remote sensing
I32	Io	10/16/2001	184	Trouble-free fly-by, high-resolution remote sensing
I33	Io	1/17/2002	102	Almost all remote sensing lost
A34	Amalthea	11/7/2002	45,800	Trailing hemisphere observations scrapped due to budget constraints
J35	Jupiter	9/21/2003	impact	

science observations at Io had to be drastically curtailed as a result of a serious tape recorder anomaly. Following the first image of the Jupiter system, the commanded tape recorder rewind failed. Telemetry showed the recorder was running but the tape was not moving. The tape recorder was the key to the LGA mission for storage of high-rate data, including the Probe data, remote sensing, and high-rate fields and particles data.

Investigation suggested that the tape was sticking to one of the heads and was slipping on the capstan. A spacecraft test on 20 October 1995 moved the tape forward for a few seconds and a comprehensive program was begun to characterize tape motion and derive a set of operating rules to minimize the chance of subsequent sticking. It was believed that the motor would always have sufficient authority in the forward direction to break the tape free. After JOI, flight software was augmented to directly control some of the recorder functions and to detect a stuck tape and stop the recorder in that event. These precautions worked well for the next 6 years, until April 2002 when the tape stuck again.

As the tape recorder investigation proceeded, project leaders had to make a painful decision regarding science observations inbound to Jupiter. Only the slowest tape speed had been demonstrated to be safe and would be sufficient to capture the one-time only Probe data acquisition as the Orbiter overflew the descending Probe. Unique fields and particles data at Io, and in the Io torus, were also benign and those observations were added to the revised science plan at little risk. Unfortunately, inbound remote sensing of Jupiter, Europa, and Io, and other high-rate data had to be eliminated from the arrival sequence. This change would maximize the chances of securing the Probe data and preserving the recorder for its now virtually essential role in *Galileo*'s orbital tour.

The magnetometer and plasma measurements during the fly-by were preserved in this adjusted science data acquisition plan, however, at a lower resolution than desired. As a result, the magnetometer measurements at JOI were inconclusive regarding the presence of an internal field, and at odds with the results of the plasma instrument (Kivelson *et al.*, 1996). The question of whether Io had an internally generated magnetic field, or whether the magnetic signal could be entirely explained by currents driven in its extended ionosphere had to wait for the acquisition of additional data. Studies of the torus using plasma waves generated in the region had to be abandoned because of the tape recorder restrictions. Sufficient data were acquired that questions of charge exchange and ion pickup between the ionosphere and the torus could be addressed in the ensuing months (Huddleston *et al.*, 1998). The intensity of current along the Io auroral footprint field lines was a surprise. Intense electron beams were found to be streaming along the Io flux tube, the cylindrical volume created by the magnetic field lines that connect Io with Jupiter. The electron beams were found to be aligned with the magnetic field and moving both up and down the field lines. Analysis showed that the electrons were accelerated in the region of Io's flux tube just above Jupiter's ionosphere and form the downward current portion of the current system associated with Io's interaction with Jupiter's co-rotating plasma. This current system is illustrated in Figure 3.1.

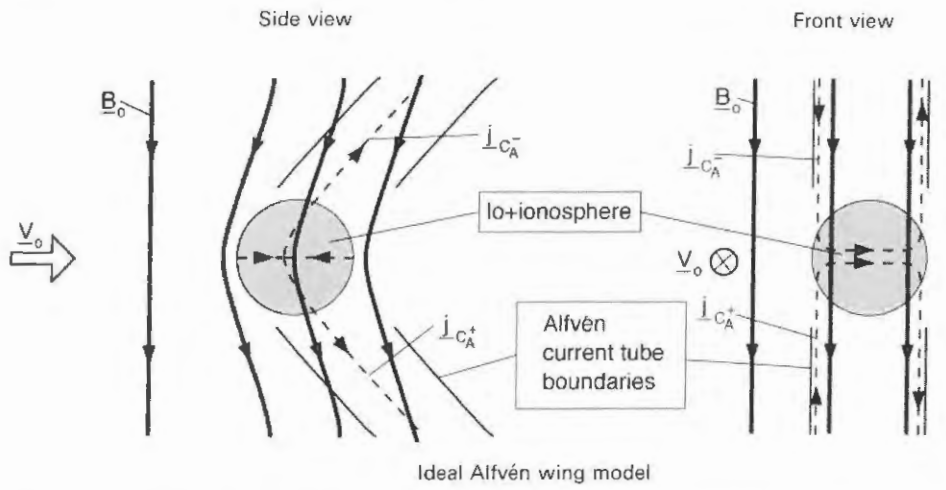

Figure 3.1. Side view and the front view of the ideal Alfvén wing model applied to Io. In the side view, Jupiter is located behind Io, in the front view Jupiter is to the far left. Magnetic field lines are bold with arrows, current flow lines are dashed with arrows, the boundaries of the current tubes are solid. Currents leaving the near-field region are connected along Alfvén characteristics to the Alfvén current tubes closing in the far-field region (after Saur *et al.*, 2004).

3.3 IO OBSERVATIONS IN THE *GALILEO* NOMINAL MISSION

Despite never coming closer than 244,000 km to Io during the nominal mission following orbit insertion, the various remote-sensing instruments on *Galileo* observed Io during almost every orbit, monitoring Io's active volcanic vents and searching for surface changes. Figure 3.2 shows a map of Io using false color images taken during the first two orbits of the *Galileo* mission. Numerous surface changes were observed between *Voyager* and *Galileo* imaging, particularly at Prometheus (new lava flow), Ra Patera (new white and yellow deposits), Euboea Fluctus (new red deposits), and Surt and Aten Paterae (*Voyager 2* plume deposits faded). Despite extensive activity observed from Earth between the *Voyager* fly-bys and the *Galileo* mission, no major surface changes were observed at Loki, Io's most energetic hot spot. As the mission progressed, some remarkable surface changes were detected, such as the change following the Pillan eruption described below.

Early *Galileo* images revealed new active volcanic centers (e.g., McEwen *et al.*, 1997, 1998a; Lopes-Gautier *et al.*, 1997, 1999), including Zamama, Gish Bar, Pillan, and Culann. *Galileo* also detected hot spots for the first time at Marduk and Prometheus, where *Voyager* had detected plumes. During the first ten orbits of *Galileo*, NIMS and SSI detected a total of 41 previously unknown hot spots (Lopes-Gautier *et al.*, 1999). The SSI was able to detect thermal emission from hot spots displaying high temperatures (>700 K) when observing Io in eclipse using its 1-μm filter, while NIMS was able to detect hot spots during both day-

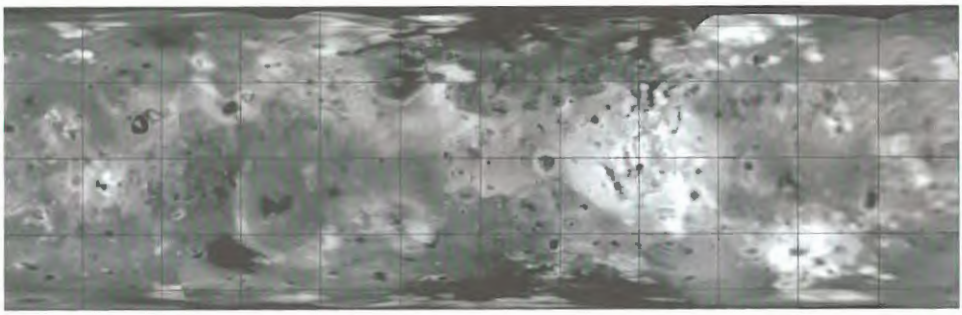

Figure 3.2. Color mosaic of images taken during the 1st and 2nd orbits during the *Galileo* nominal mission. A grid was overlain with 30° by 30° spacing. Numerous changes were observed between *Voyager* and *Galileo* but the overall pattern of volcanic centers and overall color variation was still recognizable, indicating that surface changes were limited to the area around volcanic centers that repeatedly erupted (NASA press release image PIA00585). (See also color section.)

time and night-time or eclipse observations and could detect temperatures down to about 200 K. Numerous other "suspect" spots were seen by both NIMS and SSI. Notably, SSI detected numerous bright spots at 1 μm near the sub-Jovian point of Io, however it is unclear whether those spots were active volcanic vents, local gas emissions, or something else (McEwen *et al.*, 1998a). In addition to thermal emission, SSI observations of Io in eclipse also revealed aurora produced by interactions between Io's atmosphere and plumes and the magnetospheric plasma (Geissler *et al.*, 1999).

A number of high-phase observations were also obtained during these first two orbits, allowing for imaging of Io's plume activity. A plume was found at Ra Patera during the first orbit, despite the lack of a hot spot detection by SSI (McEwen *et al.*, 1998a). Subsequent observations during the mission (by SSI, NIMS, and PPR) failed to detect a hot spot at Ra Patera until it was seen by PPR in 2001 (Rathbun *et al.*, 2004). Ra Patera was of considerable interest to investigators as, from *Voyager* images, it had caused much debate as to the nature of its flows, which were possibly sulfur (e.g., Sagan, 1979; Pieri *et al.*, 1984). By the end of the nominal mission, *Galileo* had acquired several high-phase, plume-monitoring observations. In addition, eclipse observations revealed a plume over Acala Fluctus, unseen in illuminated observations. This suggested that the Acala plume contained very little dust (McEwen *et al.*, 1998a). The high-phase observations during orbit 11, taken from distances greater than 780,000 km, revealed plumes at Zamama, Prometheus, Marduk, Pillan, and Kanehekili (Keszthelyi *et al.*, 2001).

Extensive morphological studies of volcanic features were possible during the nominal mission. Images of Io obtained during orbits 3–8 generally had higher spatial resolution than those taken during orbits 1–2, allowing for improved morphologic study of volcanic features as well as the mountains first seen in *Voyager* images. In addition, images and spectra obtained during the later portion of the *Galileo* nominal mission allowed for study of variability in Io's volcanic activity and searches for

surface changes between orbits (McEwen *et al.*, 1998a). In addition, very high phase angle images taken during the 3rd orbit showed the sodium cloud that surrounds Io (Burger *et al.*, 1999). The highest resolution images of the nominal mission were obtained during orbit 3 at distances as close as 244,000 km and have a maximum resolution of 2.5 km per pixel. These images revealed a number of mountains and other topographic features on Io's anti-Jovian hemisphere (Carr *et al.*, 1998).

The NIMS instrument was used for mapping the distribution of sulfur dioxide frost on Io, and searching for new species. Sulfur dioxide frost is ubiquitous on Io, and its spectral signature dominated the NIMS wavelength range. The only non-SO_2 component detected by NIMS during the nominal mission was the absorption feature at 3.15 μm (Carlson *et al.*, 1997), which had been previously suggested (Salama *et al.*, 1990). However, NIMS was extremely useful for studies of the global distribution of SO_2 from observations obtained during the nominal mission (Carlson *et al.*, 1997; Douté *et al.*, 2001; see also Chapter 9).

During orbits 9 and 10, SSI images were obtained at moderate-phase angle to search for surface changes, since prior orbits, and to examine mountain morphology near the terminator. The SSI also obtained eclipse observations. These observations, seen in Figure 3.3, reveal a major new eruption at the volcanic center Pillan Patera. Activity was seen by *Galileo* instruments prior to orbit 9, including a NIMS hot spot during orbits 2 and 4 (Lopes-Gautier *et al.*, 1999) and changes in caldera floor albedo from orbit to orbit (McEwen *et al.*, 1998a), but the activity was characterized as minor. However, activity at Pillan became more dramatic during late June and early July 1997 near the perijove of orbit 9. Mid-phase observations of Io by *Galileo* SSI during orbit 9 and distant observations from the Hubble Space Telescope revealed a 200 km tall plume over Pillan Patera. In addition, eclipse observations taken by *Galileo* using the clear and 1MC filter on SSI revealed a very bright spot at Pillan Patera, indicating an extremely vigorous eruption was taking place. An observation was also obtained by NIMS, closely following the SSI observation. Temperature estimates for the hot spot using both data sets indicated lava temperatures exceeding 1,700 K, higher than present-day basalt flows on Earth (McEwen *et al.*, 1998b; Davies *et al.*, 2001). This high temperature suggested an unusual composition for the lava, perhaps similar to terrestrial komatiites: ultramafic (or high-magnesium) lavas common on early Earth (Williams *et al.*, 2001; see also Chapter 7).

3.4 IO OBSERVATIONS DURING THE *GALILEO* EUROPA MISSION

Thanks in part to the amazing discoveries on Europa, NASA approved an extended mission for *Galileo* through January 2000 called the *Galileo* Europa mission (GEM). The extended mission tacked on 13 additional fly-bys to the end of the nominal mission. The first 8 orbits, 12 through 19, focused on Europa with continued distant observations of Io. The next 4 orbits, 20 through 23, were designed to reduce the perijove distance using repeated fly-bys of Callisto. This sequence included the closest approach to Io up until that point in the mission – a 140,000 km distant encounter on orbit 21. With a reduced perijove, *Galileo* was

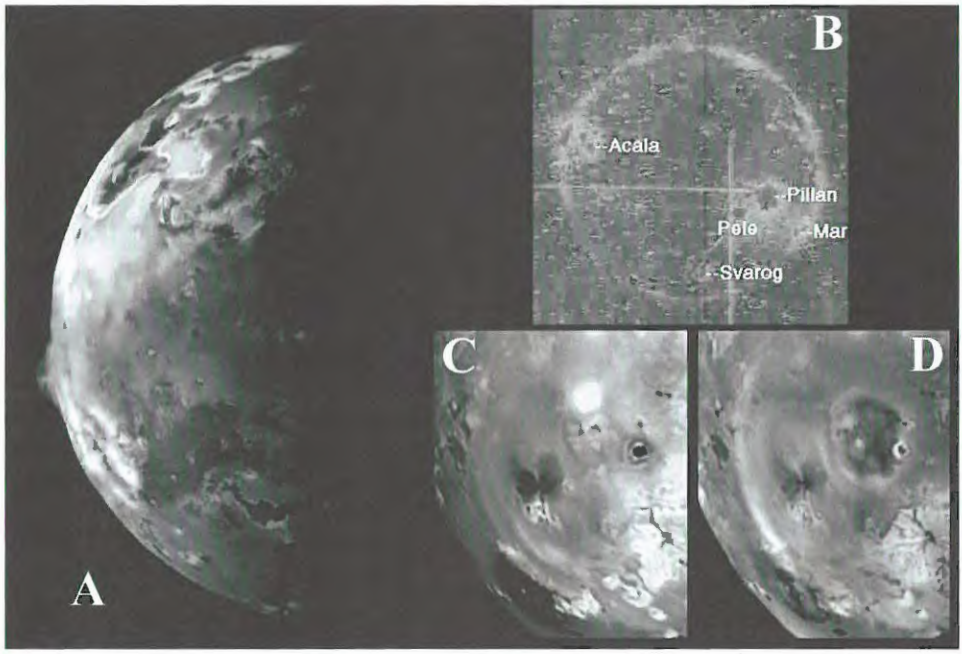

Figure 3.3. Several views of the summer 1997 eruption of Pillan Patera. North is up in all panels. (A) Shows a moderate phase angle image taken during orbit 9 (C9), showing the plume over Pillan at the limb. This observation was taken from a distance of 600,000 km and has a resolution of 6 km per pixel. (B) Shows an eclipse observation from orbit 9 showing the intensity of the Pillan eruption at the time. That observation was taken from a distance of 1.46 million kilometers and has a resolution of 14.6 km per pixel. The image has been color-coded for intensity, with red being the most intense signal. Both (C) and (D) show the aftermath of the Pillan eruption, with a new dark deposit surrounding Pillan Patera in (D). Pele and the ring that surrounds it can be seen to the south-east of Pillan. (C) Was taken during orbit 7 in April 1997 from a distance of 563,000 km, and has a resolution of 5.63 km per pixel. (D) Was taken during orbit 9 in September 1997 from a distance of 506,000 km, and has a resolution of 5.06 km per pixel (NASA press release images PIA00703, PIA01635, PIA00744). (See also color section.)

then set up to perform two close fly-bys of Io and an additional fly-by of Europa. The first Io fly-by was planned to be at 611 km (I24), and the other at 301 km, over the southern pole, and in the extended wake (I25). The question of the presence of an internally generated magnetic field could be resolved at last with a measurement over the pole. With the altitudes that were achievable, new questions arose about the possibility of actually flying through a plume.

Due to a focus on Europa, and spacecraft problems during some orbits during the Europa and Callisto phases of the GEM, SSI images of Io were only returned during orbits 14, 15, 21, and 22. During orbit 14, a clear filter image at 2.6 km per pixel was obtained by SSI showing the region surrounding Pillan (Keszthelyi *et al.*, 2001). The Pillan observation revealed the full extent of the eruption at Pillan providing the best

context view of Pillan's new lava flows. The color mosaic, shown in Figure 3.4(A) (see color section), was the highest thus far of the anti-Jovian hemisphere, showing small, previously unseen calderas with green floors, nicknamed "golf courses" and later named Chaac and Haokah Paterae (Geissler *et al.*, 1999). During orbit 15 in May 1999, three-color, high-phase observations with resolutions between 12.7 and 14 km per pixel were obtained to examine the strange photometric behavior of Io's surface materials and to search for surface changes around Kanehekili on the sub-Jovian hemisphere (Simonelli *et al.*, 2001). In addition, a four-filter, three-color eclipse observation, shown in Figure 3.3(B), was obtained to examine the interaction between the Io flux tube and Io's atmosphere and plumes (Geissler *et al.*, 1999). NIMS spectra were also obtained during orbits 12, 14, 15, 16, 20, 21, and 22. NIMS observations during this phase of the mission continued to detect hot spots, including Haokah, Susanoo, Wayland, and Girru, which had been tentatively identified from ground-based observations (Lopes *et al.*, 2001). Global or part-global observations obtained by NIMS during both the *Galileo* nominal mission and GEM linked the distribution of SO_2 to the locations of major plumes observed by SSI. Douté *et al.*'s results (2001) suggested that most of the SO_2 gas from the plumes (located mostly in the equatorial regions) flows toward colder surfaces at higher latitudes. The GEM observations also allowed the UVS to obtain its best ultraviolet observations of Io on orbit 15, providing constraints on Io's atmosphere (Hendrix *et al.*, 1999).

During orbit 21 in late June 1999, *Galileo* made its closest remote-sensing observations yet of Io, as a prelude to the Io fly-bys later that year. This fly-by allowed for an opportunity to capture a full-disk, three-color mosaic at 1.3 km per pixel, more than twice the resolution of the previous, highest resolution color observation of Io by *Galileo* during orbit 14. This mosaic, shown in Figure 3.4(C), shows the anti-Jovian hemisphere features in great detail. From the images the Amirani and Maui plumes, discovered by *Voyager*, were found to have the same vent and were in fact produced from different regions of the same, very large flow field. Other SSI results included the detection of a new plume at Masubi during orbit 21 and a dark, oval-shaped plume deposit observed during orbit 22, in August 1999, over a different location from one observed during orbit 15, indicating multiple plume sites along the long, Masubi flow field (Keszthelyi *et al.*, 2001).

3.4.1 I24

After 4 years of observing Io from a distance, *Galileo* was set to fly by Io on 11 October 1999 during orbit 24 (also known as I24). Observations from this encounter are highlighted in Figure 3.5. The fly-by was an equatorial pass, with close approach occurring near the dawn terminator north of Pillan Patera. The spacecraft came within 500 km of Io's surface. As *Galileo* receded from Io following its closest approach, a low-phase view of Io's anti-Jovian hemisphere was visible. The remote-sensing observations were designed to examine active volcanic centers, like Pillan, Prometheus, Zamama, and Amirani, to examine mountainous terrain near Dorian Montes, Tohil Mons, and Hi'iaka Patera, to examine compositional

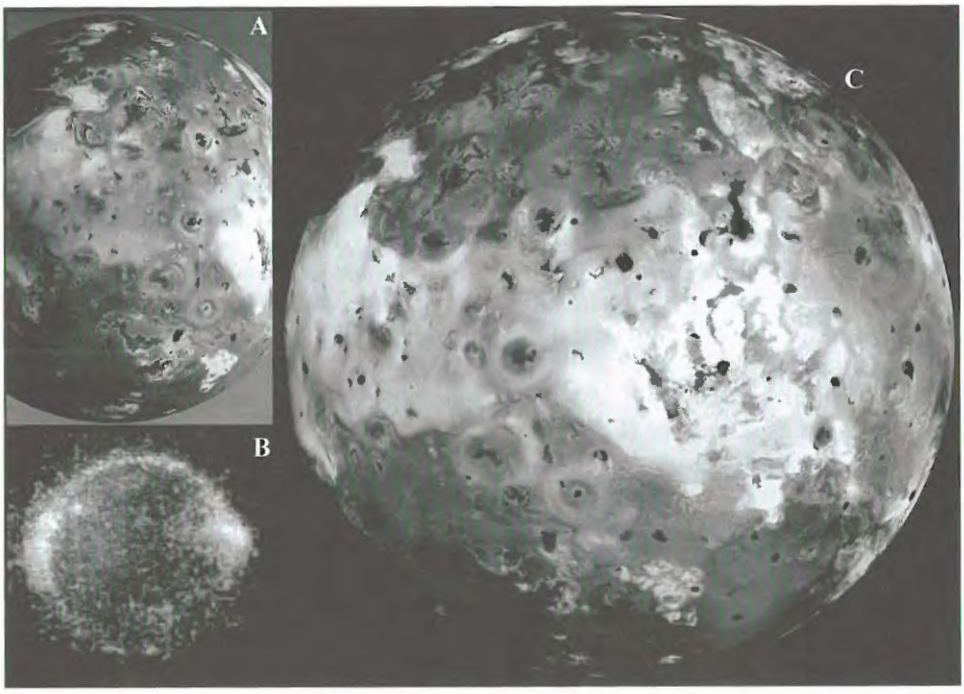

Figure 3.4. Imaging highlights from the Europa and perijove reduction phases of the GEM. (A) A mosaic of two, three-color frames showing the anti-Jovian hemisphere, taken during orbit 14 from a distance of 290,000 km with a resolution of 2.9 km per pixel. (B) A three-color observation of Io during eclipse. The faint red glows represent emissions from atomic oxygen and green glows from atomic sodium, while the bright blue emissions near the equator are likely due to electron impacts on SO_2. Image (B) was taken during orbit 15 from a distance of 1.4 million km and has a resolution of 14 km per pixel. (C) A large, three-color, 16-frame mosaic taken during orbit 21. This mosaic represents the higbest resolution view of Io by *Galileo* prior to the Io targeted encounters later in the mission. The images in this mosaic were taken from a distance of 130,000 km and have a resolution of 1.3 km per pixel (NASA press release images PIA01604, PIA01637, PIA02309). (See also color section.)

variations across the surface of Io, and to understand the thermal emission and heat flow coming from the anti-Jovian hemisphere.

The fly-by was not without its problems. A few hours before closest approach, *Galileo* went into safe mode (i.e., an anomaly caused the on-board computer to place the spacecraft into a default "safe" mode, canceling the science observation sequence), preventing observations for a few hours before close approach, but recovering in time to obtain unique, high-resolution nightside data on Loki and Pele. The SSI data acquired during this fly-by also had numerous problems (McEwen, 2001). Many of the images taken by SSI were in summation mode, with half the resolution of full-frame images. Unfortunately, these images came back garbled due to a failure in the camera electronics. An algorithm was found to unscramble the images, but some

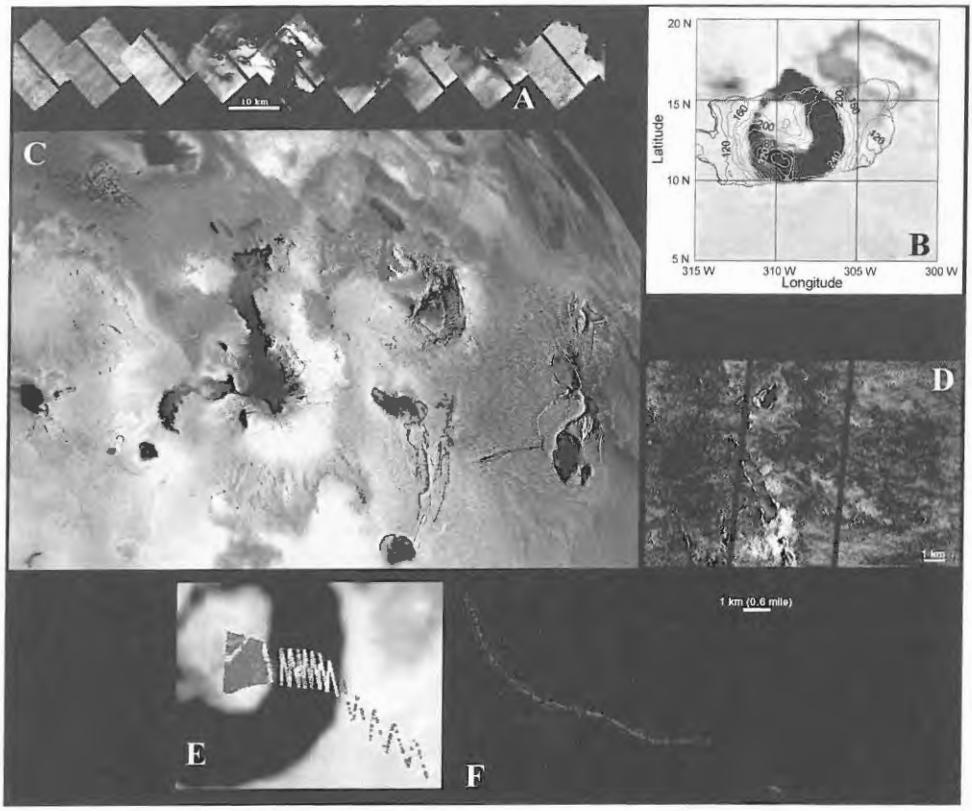

Figure 3.5. Highlights from the I24 fly-by of Io. (A) The ZAMAMA01 observation from I24. (B) Temperature map of Loki Patera taken by the PPR instrument. (C) AMSKIGI01 observation merged with color from orbit 21. (D) Portion of the PILLAN01 observation showing pits and rafted plates within the Pillan flow field. (E) NIMS observation of Loki Patera from shortly before the closest approach. (F) PELE_01 observation with a string of hot spots marking the margin of the Pele lava lake (NASA press release images PIA02537, PIA02524, PIA02526, PIA02536, PIA02514, PIA02511). (See also color section.)

artifacts, like a dark, vertical central stripe, remain. At the ends of many mosaics, partial full-resolution frames were also obtained, which were not scrambled (Keszthelyi *et al.*, 2001). NIMS also encountered problems on this fly-by. NIMS observations were designed to search for compositional variations as well as look at the high-resolution structure of volcanic hot spots. Unfortunately, the instrument's grating, which had been losing effectiveness through the GEM, became stuck in one position, allowing for spectra from only 13 wavelengths to be obtained. Luckily, the wavelengths were widely spaced within the NIMS full spectral range, but the spectral resolution achieved by only having 17 wavelengths available over a range of more than 4 μm would not be enough to resolve any but the broadest of spectral

features (Lopes-Gautier *et al.*, 2000; Lopes *et al.*, 2001). The spectral resolution would be enough, however, to search for hot spots, determine temperatures, and map the SO_2 distribution.

The SSI team obtained 12 clear-filter mosaic sequences for I24, many suffering from the problems associated with the summation mode. These observations are discussed in further detail in Keszthelyi *et al.* (2001) and Turtle *et al.* (2001). In addition to SSI imaging, both NIMS and PPR obtained critical, high-resolution data during the I24 fly-by, despite the NIMS grating problem. NIMS regional observations revealed 16 hot spots, 3 not previously seen. In addition, high-resolution data of Loki (shown in Figure 3.5(E)), Prometheus, and Amirani revealed a high-resolution structure to the hot spots (including multiple hot spots in the same flow field) not previously resolved (Lopes *et al.*, 2001). A correlation was also found between red plume deposits and enhanced concentrations of SO_2 (Lopes-Gautier *et al.*, 2000). PPR obtained high spatial resolution observations of temperatures on the floors of Loki (shown in Figure 3.5(B)) and Pele, as well as the flow fields of Pillan (Spencer *et al.*, 2000; Rathbun *et al.*, 2004).

I24 also enabled plasma wave studies of radio emissions at Io akin to terrestrial Auroral Kilometric Radiation (AKR) (Gurnett *et al.*, 2001). Such emissions are a response to changing energetic particle distribution functions in the region, which were also studied by the EPD instrument. Behaviors of distribution functions are in turn related to the dynamics of particle responses to changing electric and magnetic field conditions. PLS investigators suggested that the spacecraft went through a "stealth plume" – a cloud of material over Pele at an altitude of 600 km (Frank and Paterson, 2000). Taken together these measurements were a first attempt at characterizing the complex relationships and dynamics in the Jovian inner magnetosphere driven by Io surface conditions.

3.4.2 I25

Following the problems encountered during the I24 fly-by, SSI observations for the I25 fly-by were quickly replanned to eliminate the offending summation mode images. Because full-mode images take up around four times as much memory as summation mode images, fewer images had to be planned. The I25 fly-by, on 26 November 1999, was a south polar pass, at an altitude of 300 km, designed to investigate the magnetic signature found by the magnetometer during the Io fly-by during JOI as well as to examine polar terrain that had not been observed thus far by *Galileo*. Unfortunately, the spacecraft went into safe mode less than 5 hours before the I25 closest approach. With a 34 minute one-way-light-time, the JPL engineering team had a total of three and a half hours to respond in order to recover science observations during the encounter. The team created a bare-bones sequence in which many instruments were not able to participate. One particularly important instrument that was not recovered was the magnetometer. The recovery process completed 4 minutes before the new sequence went active. All images with pixel scales less than 150 m per pixel were lost as well as any other data taken before and shortly after closest approach (Turtle *et al.*, 2001). Despite losing the highest resolution images, the images that were

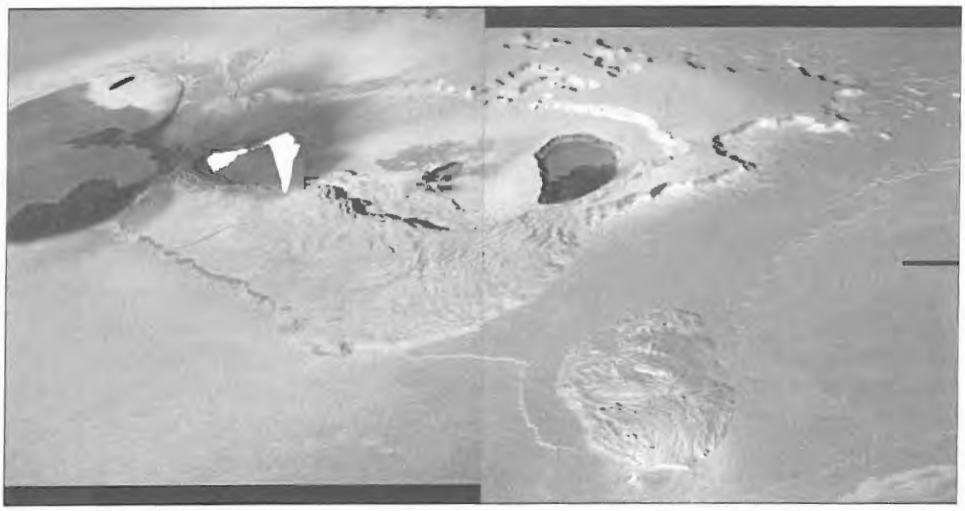

Figure 3.6. Two-frame mosaic from the GIANTS01 observations from I25. This observation shows Tvashtar Paterae at 180 m per pixel. The bright features seen in the left image are due to saturation of the detector (and subsequent bleeding) caused by a brilliant thermal emission source. Based on the morphology of the saturation, the source was interpreted as a vigorous lava curtain, with lava flow on the surface away from the curtain (McEwen *et al.*, 2000).

taken had much higher quality than those of the I24 summation mode images and were much more useful for geologic interpretation. SSI images included mosaics of Zal Patera and Montes, Hi'iaka Patera and Montes, Tvashtar Paterae, and Emakong Patera.

One of the biggest surprises of the Io fly-bys was the major eruption at Tvashtar Paterae. An SSI mosaic was planned over Tvashtar Paterae. This observation, a two-frame mosaic with a resolution of 183 m per pixel (Figure 3.6), was designed to study a group of calderas at high northern latitudes that are much larger than the average Ionian calderas nearer the equator. Unexpectedly, one of the nested calderas within Tvashtar Paterae erupted during the I25 fly-by. Intense thermal emission from a long fire fountain saturated the SSI detector (McEwen *et al.*, 2000). The eruption was also seen in observations taken by NIMS as well as by ground-based observers (Lopes-Gautier *et al.*, 2000; Howell *et al.*, 2001). Ground-based observers measured the temperature at between 1,300 K and 1,900 K, while NIMS and SSI placed constraints of 1,060 K and at least 1,300 K (Lopes *et al.*, 2001; Milazzo *et al.*, 2005).

Like SSI, NIMS and PPR data were limited to lower resolution data over the sunlit anti-Jovian hemisphere. Regional observations by NIMS detected three new hot spots at Cuchi, Chaac, and Seth Paterae (Lopes *et al.*, 2001). PPR obtained part of a high-quality global map of night-time thermal emission on approach, before being interrupted by the safing of the spacecraft (Spencer *et al.*, 2000a).

The fields and particles instruments also suffered significant observation losses, including the magnetometer measurements and plasma measurements in the Io exosphere. However, an important set of measurements conducted by PWS

showed for the first time the presence of very large electron densities of up to $6.8 \times 10^4\,\mathrm{cm}^{-3}$ in an extended plasma wake of Io, and over the southern polar region of Io (Gurnett *et al.*, 2001). The enhanced electron densities over the southern polar region had a nearly rectangular profile, the edges of which coincided with the boundaries of the Io flux tube, apparently due to the diffusion of plasma outward away from Io along the flux tube. These measurements shed light on the flux interchange mechanism that drives plasma from the vicinity of Io down the magnetotail of Jupiter.

3.5 IO OBSERVATIONS DURING THE *GALILEO* MILLENNIUM MISSION

The original plan for the GEM called for only two fly-bys of Io, I24 and I25, with the expectation that the spacecraft would have significant problems following two passes through the Io plasma torus. However, the spacecraft survived intact, even though several instruments were not functioning optimally. So an additional Io fly-by was approved for orbit 27 (I27) on 22 February 2000 as well as two additional fly-bys of Ganymede in May and December 2000 as part of a new extended mission called the *Galileo* millennium mission (GMM). These were followed by three final Io fly-bys (I31–I33) in 2001–2002. GMM took advantage of the opportunity in late 2000 to study the magnetosphere of Jupiter with two spacecraft, *Galileo* in the magnetosphere of Jupiter, and *Cassini* while on the way to its historic encounter with Saturn, passing by on the dayside. Among other things, *Cassini* was able to monitor solar wind conditions for comparison with *Galileo*'s magnetospheric observations, to look for the influence of the solar wind on the magnetosphere.

Among the priorities for Io investigations were more measurements to determine the nature of any intrinsic magnetic field of Io. In GMM, Io polar fly-bys would be performed in order to detect the differences an intrinsic magnetic field would introduce between the equatorial magnetic field and the polar magnetic field. I31 provided the first close pass of the north polar region, I32 would pass over the south pole (where observations were lost in I25). Extensive remote-sensing observations were also planned, with the intention of tripling the high-resolution data (<200 m per pixel) coverage for Io. After I33, the spacecraft would be on a ballistic trajectory for a Jupiter impact on the 35th orbit. Imaging would be turned off for A34 and J35.

The *Galileo* Millennium Mission (GMM) provided key opportunities for the fields and particles instruments. The collective studies of a body of encounters with Io, including studies of the extended corona, would provide an understanding of the patchy nature of the atmosphere; the composition, properties, and dynamics of the Io flux tube and its interaction with the atmosphere of Jupiter; the interaction of the atmosphere with the torus; and the mechanics of how Iogenic plasma spreads throughout the Jovian magnetosphere. The Io encounters in GMM were performed at a range of local times and geometries with respect to the Io wake. The coordinated study of Jupiter's magnetosphere with *Cassini* showed two main results. First, there seem to be globally correlated dynamic events in the magnetosphere and the signature

of these events can be seen in a number of data sets: energetic particle events, injection events, changes in hectometric, narrowband kilometric, and trapped continuum radiation. It is as if the magnetotail undergoes a global reconfiguration from time to time (Vasyliunas *et al.*, 1997; Krupp *et al.*, 2001a, b, 2004). Second, this set of events does not seem to be correlated with solar wind variations at Jupiter (Kurth *et al.*, 2002). The absence of a correlation with solar wind suggests that the magnetosphere may exhibit a systematic response to the presence of Iogenic plasma.

3.5.1 I27

The I27 fly-by was an equatorial pass with a similar geometry to the I24 fly-by. *Galileo* also came much closer to Io on this pass, flying within 200 km of the surface. Unlike the previous two fly-bys, where problems due to the various instruments or due to "safing" events occurred on the spacecraft, this fly-by went without a glitch and all planned data was obtained. This encounter also provided a fly-through of the Io torus. Intense ion cyclotron wave activity on this and other encounters provided measurements to confirm the extensive nature of the charged particle pickup activity in the region, a level of activity that results in the spread of Iogenic material, an order of magnitude beyond the 2-Io radii originally supposed.

SSI took a number of observation sequences, including repeat observations of Pele, Prometheus, Tohil Mons, Tvashtar Paterae, Amirani, and Zal Patera. Additional observations were planned for a cliff near Isum Patera, Chaac Patera and its surrounding region, Shamshu Patera and Mons, and near Telegonus Mensae. NIMS and PPR, like SSI, were able to acquire all of their planned data. Much of the NIMS and PPR data were designed to provide ride-along coverage with SSI, allowing for correlation between the data sets. Among the highlights for NIMS include a high-resolution observation of Pele, shown in Figure 3.7(B), finding a correlation between dark material and thermal emissions in the Chaac–Camaxtli region, the discovery of four new hot spots in regional observations, and the study of the detailed thermal structure of the Amirani and Prometheus flow fields (Lopes *et al.*, 2001). NIMS data from I24–I27 were also used to map the SO_2 distribution around Prometheus. Douté *et al.* (2002) used the SO_2 distribution to infer the migration of the Prometheus plume over Io's surface, a concept first proposed by Kieffer *et al.* (2000). PPR, in addition to providing ride-along data with SSI, observed its first global night-time map, covering the trailing hemisphere, shown in Figure 3.7(C), to look for sites of low-temperature thermal emission and to determine background surface temperatures. It also obtained high-resolution observations of Loki, showing dramatic changes since I24, and regional maps of dayside thermal emission (Spencer *et al.*, 2000a; Rathbun *et al.*, 2004).

3.5.2 G29–I31

During orbit 29 in late December 2000, *Galileo* and *Cassini* obtained complimentary coverage of Io, with *Cassini* providing better spectral and temporal coverage thanks to its more sophisticated imaging system and higher bandwidth and *Galileo* providing

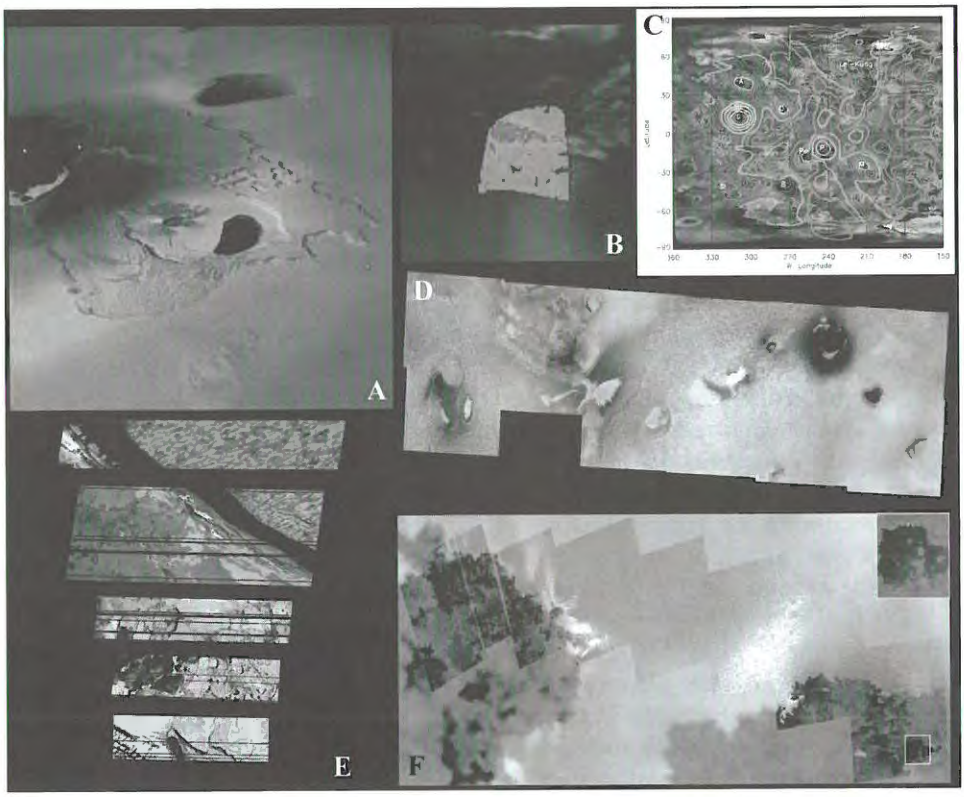

Figure 3.7. Highlights from the I27 fly-by. (A) False-color view of Tvashtar Paterae from the TVASHT01 observation. (B) NIMS observation of the Pele caldera overlain on a false-color image from *Voyager 1*. (C) Map of night-time temperatures of Io's trailing hemisphere taken by the PPR instrument. (D) CAMAXT01 observation merged with color from orbit 21. (E) Partial frames from the CHAAC01 observation. Frames showing the north-east margin of Chaac Patera are seen at the top while frames showing the floor and the south-west margin are seen at the bottom. (F) PROMTH01 observation. A dark flow with two spots of incandescent lava is highlighted to the right (NASA press release images PIA02550, PIA02560, PIA02548, PIA02566, PIA02551, PIA02564). (See also color section.)

better spatial coverage since it observed Io from a much closer distance. *Cassini* observations, shown in Figure 3.8(A), revealed a new plume at Tvashtar Paterae, one of the few found over a polar region (Porco *et al.*, 2003). Low-phase *Galileo* color observations, with resolutions between 11 and 17 km per pixel (shown in Figure 3.8(B)), revealed a red plume deposit, similar to that seen around Pele, surrounding Tvashtar, forming a ring 1,440 km across (Turtle *et al.*, 2004).

Following orbit 29, the spacecraft continued to perform well, except for an anomaly that cropped up, starting in orbit 28, which caused the loss of a number of SSI images. A further extension mission was granted, including a fly-by of *Callisto* in May 2001, three fly-bys of Io in August and October 2001 and January 2002, and a

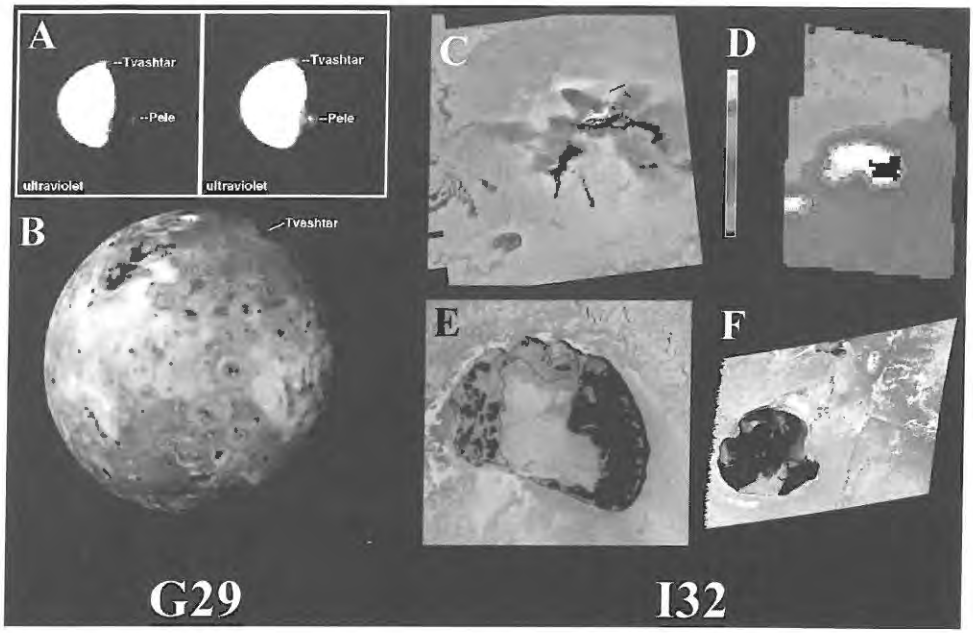

Figure 3.8. Highlights from orbit 29 and I32. Both (A) and (B) highlight a new eruption at Tvashtar observed during late 2000. The two figures in (A), enhanced images from the *Cassini* spacecraft, show a 385 km tall plume over Tvashtar as well as the plume over Pele. As seen in (B) from *Galileo*, both plumes have formed large red ring deposits. Panels (C–F) show highlights from the I32 fly-by. Both (C) and (D) show a new eruption at Thor, first seen by NIMS during I31 and in distant observations from the same orbit. Image (C) is taken from the TERMIN02 observation while (D) is a 13–16 km per pixel observation from NIMS. (E) Color observation of Tupan Patera, from the observation TUPAN_01. (F) Frame from the observation GSHBAR01, revealing fresh lava flows on its surface. (See also color section.)

fly-by of Amalthea in November 2002. Following the Amalthea fly-by, *Galileo* would then be put on a collision course with Jupiter, to prevent contamination of Europa from potential microbial stowaways on *Galileo*. Observations during the first orbit of this new extension mission, orbit 30, were designed to look at the anti-Jovian and leading hemispheres at low-phase to search for changes, examine the new Tvashtar plume deposit found during Orbit 29, and to characterize the volcanic features seen near 50° west longitude which had not been well observed by *Galileo* (or *Voyager* for that matter). Unfortunately, the SSI anomaly that started in orbit 28 occurred again during orbit 30, causing the loss of all orbit 30 images of Io.

I31 was a north polar fly-by of Io that took place on 6 August 2001. Closest approach occurred at a distance of 194 km above the surface of Io near 78° north latitude, 172° west longitude. Magnetometer measurements were performed and the results were particularly important, as they demonstrated that there is no internally generated magnetic field at Io. At a fly-by altitude of only 194 km, the spacecraft

trajectory took it directly over Tvashtar, which had been recently active. Images and spectra showed that Tvashtar was probably quiescent at the time of *Galileo*'s overflight. Nevertheless, detections by the PLS instrument of tenuous gases in the area indicated that another plume was active, and represent the first *in situ* detection of its kind of emissions from an active region not on Earth.

Imaging plans called for high-resolution observations of the I25 Tvashtar eruption site and other features (Turtle *et al.*, 2004). Unfortunately, despite commands designed to fix the SSI anomaly seen since orbit 28, the problem appeared again, causing the loss of all SSI images except the low-resolution observations. These observations, combined with those taken by NIMS, revealed a major new eruption at a volcano later named Thor. SSI observations at 18 km per pixel prior to the encounter revealed a 500 km tall plume over Thor, the tallest plume ever seen at Io in reflected sunlight (Turtle *et al.*, 2004). It quickly became clear that this was the plume whose gases were sampled by the PLS instrument. Low-resolution images of Thor during this fly-by revealed a new dark deposit surrounded by a white plume deposit, where no major activity or dark material was seen previously (Geissler *et al.*, 2004). NIMS regional observations revealed a strong thermal emission source at Thor during I31 (Lopes *et al.*, 2004) which pinpointed the location of the erupting plume. NIMS observations also revealed nine additional, previously undetected hot spots. Despite not seeing a plume or new plume deposit in the polar regions of Io during much of the *Galileo* mission (save perhaps one possible north polar detection in 1997), SSI low-resolution observations also revealed a new red ring plume deposit around Dazhbog Patera and additional red plume deposits at Surt, in addition to the deposits surrounding Tvashtar first seen on orbit 29 (Geissler *et al.*, 2004). This brought the total of plume deposits north of 40° north latitude to four in only a matter of a few months, where maybe only one had been seen during the rest of the mission. PPR obtained global and regional maps of nightside thermal emission from the volcanoes and passive surface, and its best-ever map of daytime thermal emission and surface temperatures (Rathbun *et al.*, 2004).

3.5.3 I32

The I32 encounter was a south polar fly-by of Io that took place on 16 October 2001. Closest approach occurred at a distance of 184 km above the surface of Io near 79° south latitude, 223° west longitude. Once again, this encounter provided a look at the anti-Jovian hemisphere of Io. The anomaly that caused the loss of high-resolution SSI images during I31 did not happen this time. Thus, all planned SSI observations for this fly-by were successfully obtained. Among the highlights of this fly-by was the chance to retarget observations to the location of the eruption at Thor, seen during the previous encounter. SSI obtained images at 335 m per pixel near the terminator in the northern hemisphere, which included Thor. The frame showing Thor, shown in Figure 3.8(D), shows two separate dark lava flows covering brightened flows from previous eruptions. Surrounding the dark flows is a dark pyroclastic deposit, similar to the one seen at Pillan and Pele (Turtle *et al.*, 2004). NIMS also captured a high-resolution observation, at 13–16 km per pixel, of the newly discovered

hot spot, shown in Figure 3.8(D), revealing continued activity at Thor along with a newly detected hot spot to the south-west of Thor, suggesting the presence of multiple vents for the same internal source region (Lopes *et al.*, 2004).

NIMS obtained several observations in conjunction with SSI observations as well as several regional coverage observations, including a night-time observation of the southern portion of Loki Patera having a broader spatial coverage than the observation during I24. The highest thermal emission was seen along the south-western edge of Loki Patera, a region known to be the starting point of repeated eruptions at Loki. NIMS data showed that several other Ionian paterae, including Tupan and Emakong, are likely to be persistent lava lakes, a result that has important implications for the resurfacing of Io (Lopes *et al.*, 2004), which may be primarily due to plume deposits rather than lava flows (Geissler *et al.*, 2004). During I32, PPR again obtained global and regional maps of night-time thermal emission (Rathbun *et al.*, 2004).

Further magnetometer measurements obtained during this fly-by confirmed that there is no internally generated magnetic field at Io. This encounter also included a first-time penetration of a peculiar region near Io known as the Io ramp. The ramp is a transition region from the relatively cold plasma of magnetospheric origin to the more energetic plasma of Io torus origin. Density and energy of plasma increase sharply in this transition. *Galileo* was able to obtain a nearly 2-hour sample in this region.

3.6 THE END OF THE *GALILEO* MISSION

The I33 fly-by, on 17 January 2002, was *Galileo*'s closest encounter with Io, with an altitude of only 102 km. This fly-by was also tbe only one to provide a high-resolution view of Io's Jupiter-facing hemisphere. Unfortunately, a "safing" event occurred shortly before the encounter and all Io data for the fly-by was lost except for some small maps of night-time thermal emissions from PPR. Additional observations were planned for orbit 34, in November 2002, when *Galileo* would come within 50,000 km of Io. This fly-by would have provided *Galileo*'s best look in daylight at prominent volcanic centers like Loki, Pillan, Ra Patera, and Pele. However, due to budget constraints, no remote-sensing observations of Io were performed during orbit 34.

The I33 encounter provided a rare opportunity to sample another peculiar region near Io known as the Io ribbon. The ribbon, as seen from the ground, is a tenuous energetic region located between the cold and warm plasma torii (Figure 3.9). Unfortunately, 5 minutes into this recording, the spacecraft went into "safing event", and this measurement was lost. The A34 and J35 sequences were designed to obtain the measurements that would establish the flux tube interchange mechanism as the controling mechanism for large-scale movement of plasma from Io to other regions of the Jovian magnetosphere. In this mechanism, flux tubes, heavily mass loaded with Iogenic plasma would be moved out by centrifugal force and replaced with comparatively empty flux tubes moving inward. Evidence for this process was sought in the *Voyager* data, but these efforts were generally unsuccessful. Extensive observations of the inner magnetosphere by *Galileo* early in the mission were the first

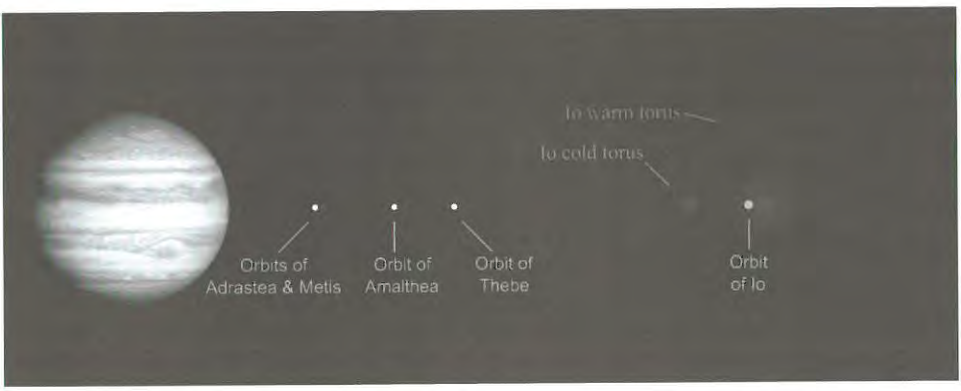

Figure 3.9. This figure illustrates both the warm and cold torus of Io. The *Galileo* spacecraft was able to sample the cold torus on the 34th orbit of Jupiter just before its final trajectory loop around Jupiter on J35. Courtesy Windows to the Universe *www.windows.ucar.edu* A34 Interactive Graphic. (See also color section.)

evidence that this process worked at Jupiter. Additional measurements during GMM, including those on A34, helped to establish the viability of this mechanism. The A34 trajectory provided the first penetration to the cold torus of Io, and *Galileo* obtained the first *in situ* measurements of that region.

Following perijove on orbit 34, *Galileo* was on a collision course, and on 23 September 2003, *Galileo* followed its atmospheric probe into Jupiter's atmosphere, ending the *Galileo* mission. Despite numerous problems with the antenna and tape recorder before the start of the primary mission, and radiation-related problems during the extended mission, *Galileo* provided critical insights into the geology and inner workings of Io. Whereas *Voyager* provided a first look at world known until then as a point in a telescope or a spectrometer plot, *Galileo* brought Io up close and personal, allowing researchers to examine the fine-scale geology, chemistry, and physics of this fascinating world.

3.7 REFERENCES

Anderson, J. D., Sjogren, W. L., and Schubert, G. 1996. Galileo gravity results and the internal structure of Io. *Science*, **272**, 709–712.

Belton, M. J. S., Klaasen, K. P., Clary, M. C., Anderson, J. L., Anger, C. D., Carr, M. H., Chapman, C. R., Davies, M. E., Greeley, R., Anderson, D. *et al.* 1992. The Galileo solid-state imaging experiment. *Space Sci. Rev.*, **60**, 413–455.

Burger, M. H., Schneider, N. M., and Wilson, J. K. 1999. Galileo's close-up view of the Io sodium jet. *Geophys. Res. Lett.*, **26**, 3333–3336.

Carlson, R. W., Weissman, P. R., Smythe, W. D., and Mahoney, J. C. 1992. The Near-Infrared Mapping Spectrometer Experiment on Galileo. *Space Science Reviews*, **60**, 457–502.

Carlson, R., Smythe, W., Lopes-Gautier, R., *et al.* 1997. The distribution of sulfur dioxide and other infrared absorbers on the surface of Io in 1997. *Geophys. Res. Lett.*, **24**(20), 2474–2482.

Carr, M. H., McEwen, A. S., Howard, K. A., Chuang, F. C., Thomas, P., Schuster, P., Oberst, J., Keukum, G., Schubert, G., and the Galileo Imaging Team. 1998. Mountains and calderas on Io: Possible implications for lithosphere structure and magma generation. *Icarus*, **1935**, 146–165.

Davies, A. G., Keszthelyi, L. P., Williams, D. A., Phillips, C. B., McEwen, A. S., Lopes, R. M. C., Smythe, W. D., Kamp, L. W., Soderblom, L. A., and Carlson, R. W. 2001. Thermal signature, eruption style, and eruption evolution at Pele and Pillan on Io. *Journal of Geophys. Res.*, **106**, 33079–33103.

Douté, S., Lopes-Gautier, R., Carlson, R., Schmitt, B., Soderblom, L., and the Galileo NIMS Team. 2001. Mapping the SO_2 frost on Io by the modeling of NIMS hyperspectral images. *Icarus*, **149**, 107–132.

Doute; S., Lopes, R., Kamp, L. W., and Carlson, R. 2002. Dynamics and evolution of SO_2 Gas condensation around Prometheus-like volcanic plumes on Io as seen by the Near-Infrared Mapping Spectrometer. *Icarus*, **158**, 460–482.

Douté, S., Lopes, R., Kamp, L. W., Carlson, R. W., Schmitt, B., and the Galileo NIMS Team. 2004. Geology and activity around volcanoes on Io from the analysis of NIMS spectral images. *Icarus*, **169**(1), 175–196.

Frank, L. A. and Paterson, W. R. 2000. Return to Io by the Galileo spacecraft – Plasma observations. *Journal of Geophys. Res.*, **105**, 25363–25378.

Geissler, P. E., McEwen, A. S., Ip, W., Belton, J. S., Johnson, T. V., Smythe, W. H., and Ingersoll, A. P. 1999. Galileo imaging of atmospheric emissions from Io. *Science*, **285**, 870–874.

Geissler, P., McEwen, A. S., Phillips, C. B., Keszthelyi, L. P., and Spencer, J. 2004. Surface changes on Io during the Galileo mission. *Icarus*, **169**, 2964.

Gurnett, D. A., Persoon, A. M., Kurth, W. S., Roux, A., and Bolton, S. J. 2001. Electron densities near Io from Galileo plasma wave observations. *Journal of Geophys. Res.*, **106**, 26225–26232.

Harland, D. M. 2000. *Jupiter Odyssey: The Story of NASA's Galileo Mission*. Springer, London.

Hendrix, A. R., Stewart, A. I. F., Simmons, K. E., and Tobiska, W. K. 1999. Galileo ultraviolet spectrometer observations of Io: Spatial and temporal variations in sulfur dioxide gas and frost. *EOS*, **80**, F623.

Howell, R. R., Spencer, J. R., Goguen, J. D., Marchis, F., Prangé, R., Fusco, T., Blaney, D. L., Veeder, G. J., Rathbun, J. A., Orton, G. S., *et al.* 2001. Ground-based observations of volcanism on Io in 1999 and early 2000. *Journal of Geophys. Res.*, **106**, 33129–33139.

Huddleston, D. E., Strangeway, R. J., Warnecke, J., Russell, C. T., and Kivelson, M. G. 1998. Ion cyclotron waves in the Io torus: Wave dispersion, free energy analysis, and SO2 + source rate estimates. *Journal of Geophysical Research-Planets*, **103**, 19887–19899.

Keszthelyi, L., McEwen, A. S., Phillips, C. B., Milazzo, M., Geissler, P., Turtle, E. P., Radebaugh, J., Williams, D. A., Simonelli, D. P., Breneman, H. H., *et al.* 2001. Imaging of volcanic activity on Jupiter's moon Io by Galileo during the Galileo Europa Mission and the Galileo Millennium Mission. *Journal of Geophys. Res.*, **106**, 33025–33052.

Kieffer, S. W., Lopen-Gautier, R., McEwen, A., Smythe, W., Keszthelyi, L., and Carlson, R. 2000. Prometheus: Io's wandering plume. *Science*, **288**, 1204–1208.

Kivelson, M. G., Khurana, K. K., Walker, R. J., Linker, J. A., Russell, C. T., Southwood, D. J., and Polanskey, C. 1996. A magnetic signature at Io: Initial report from the Galileo magnetometer. *Science*, **273**, 337–340.

Krupp, N., Vasyliunas, V. M., Woch, J., Lagg, A., Khurana, K. K., Kivelson, M. G., Mauk, B. H., Roelof, E. C., Williams, D. J., Krimigis, S. M. *et al.* 2004. Dynamics of the Jovian Magnetosphere. In: F. Bagenal, T. Dowling, and W. McKinnon (eds.), *Jupiter: The Planet, Satellites, and Magnetosphere*. Cambridge University Press, Cambridge, UK, pp. 617–638.

Krupp, N., Lagg, A., Wilken, B., Woch, J., Livi, S., Roelof, E. C., and Williams, D. J. 2001. Global flows of energetic ions in Jupiter's equatorial plane – First-order approximation. *Journal of Geophys. Res. A. Space Physics*, **106**, 26017–26032.

Krupp, N., Woch, J., Lagg, A., Roelof, E. C., Williams, D. J., Livi, S., and Wilken, B. 2001. Local time asymmetry of energetic ion anisotropies in the Jovian magnetosphere. *Planetary and Space Science*, **49**, 283–289.

Kurth, W. S., Gurnett, D. A., Hospodarsky, G. B., Farrell, W. M., Roux, A., Dougherty, M. K., Joy, S. P., Kivelson, M. G., Walker, R. J., Crary, F. J., *et al.* 2002. The dusk flank of Jupiter's magnetosphere. *Nature*, **415**, 991–994.

Lopes, R. M. C., Kamp, L. W., Douté, S., Smythe, W. D., Carlson, R. W., McEwen, A. S., Geissler, P. E., Kieffer, S. W., Leader, F. E., Davies, A. G. *et al.* 2001. Io in the near infrared: Near-Infrared Mapping Spectrometer (NIMS) results from the Galileo flybys in 1999 and 2000. *Journal of Geophys. Res.*, **106**, 33053–33078.

Lopes, R. M. C., Kamp, L. W., Smythe, W. D., Mouginis-Mark, P., Kargel, J., Radebaugh, J., Turtle, E. P., Perry, J., Williams, D. A., Carlson, R. W., *et al.* 2004. Lava lakes on Io: Observations of Io's volcanic activity from Galileo NIMS during the 2001 fly-bys. *Icarus*, **169**, 140–174.

Lopes-Gautier, R., Davies, A. G., Carlson, R., Smythe, W., Kamp, L., Soderblom, L., Leader, F. E., Mehlman, R., and the Galileo NIMS Team. 1997. Hot Spots on Io: Initial results from Galileo's Near Infrared Mapping Spectrometer. *Geophys. Res. Lett.*, **24**(20), 2439–2442.

Lopes-Gautier, R., McEwen, A. S., Smythe, W. B., Geissler, P. E., Kamp, L., Davies, A. G., Spencer, J. R., Keszthelyi, L., Carlson, R., Leader, F. E., *et al.* 1999. Active volcanism on Io: Global distribution and variations in activity. *Icarus*, **140**, 243–264.

Lopes-Gautier, R., Douté, S., Smythe, W. D., Kamp, L. W., Carlson, R. W., Davies, A. G., Leader, F. E., McEwen, A. S., Geissler, P. E., Kieffer, S. W. *et al.* 2000. A close-up look at Io from Galileo's Near-Infrared Mapping Spectrometer. *Science*, **288**, 1201–1204.

McEwen, A. S. 2001. Introduction to the special section: Geology and geophysics of Io. *Journal of Geophys. Res.*, **106**, 32959–32961.

McEwen, A. S., Simonelli, D. P., Senske, D. R., Klassen, K. P., Keszthelyi, L., Johnson, T. V., Geissler, P. E., Carr, M. H., and Belton, M. J. S. 1997. High-temperature hot spots on Io as seen by the Galileo solid state imaging (SSI) experiment. *Geophys. Res. Lett.*, **24**(20), 2443–2446.

McEwen, A. S., Keszthelyi, L., Geissler, P., Simonelli, D. P., Carr, M. H., Johnson, T. V., Klaasen, K. P., Breneman, H., Jones, T. J., Kaufman, J. M., *et al.* 1998a. Active volcanism on Io as seen by Galileo SSI. *Icarus*, **135**, 181–219.

McEwen, A. S., Keszthelyi, L., Spencer, J. R., Schubert, G., Matson, D. L., Lopes-Gautier, R., Klassen, K. P., Head, J. W., Geissler, P., Fagents, S. *et al.* 1998b. High temperature silicate volcanism on Jupiter's moon Io. *Science*, **281**, 181–219.

McEwen, A. S., Belton, M. J. S., Breneman, H. H., Fagents, S. A., Geissler, P., Greeley, R., Head, J. W., Hoppa, G., Jaeger, W. L., Johnson, T. V. *et al.* 2000. Galileo at Io: Results from high-resolution imaging. *Science*, **288**, 1193–1198.

Milazzo, M. P., Keszthelyi, L. P., Radebaugh, J., Davies, A. G., Turtle, E. P., Geissler, P. E., Klaasen, K. P., Rathbun, J. A., and McEwen, A. S. 2005. Volcanic activity at Tvashtar Catena, Io. *Icarus*, **179**, 235–251.

Pieri, D. C., Baloga, S. M., Nelson, R. M., and Sagan, C. 1984. Sulfur flows on Ra Patera, Io. *Icarus*, **60**, 685–700.

Porco, C. C., and 23 colleagues. 2003. Cassini imaging of Jupiter's atmosphere, satellites, and rings. *Science*, **299**, 1541–1547.

Rathbun, J. A., Spencer, J. R., Tamppari, L. K., Martin, T. Z., Barnard, L., and Travis, L. D. 2004. Mapping of Io's thermal radiation by the Galileo photopolarimeter–radiometer (PPR) instrument. *Icarus*, **169**, 127–139.

Russell, E. E., Brown, F. G., Chandos, R. A., Fincher, W. C., Kubel, L. F., Lacis, A. A., and Travis, L. D. 1992. Galileo photopolarimeter/radiometer experiment. *Space Sci. Rev.*, **60**, 531–563.

Sagan, C. 1979. Sulphur flows on Io. *Nature*, **280**, 750–753.

Salama, F., Allamandola, L. J., Witteborn, F. C., Cruikshank, D. P., Sandford, S. A., and Bregman, J. D. 1990. The 2.5–5.0 μm spectra of Io: Evidence for H_2S and H_2O frozen in SO_2. *Icarus*, **83**, 66–82.

Saur, J., Neubauer, F. M., Connerney, J. E. P., Zarka, P., and Kivelson, M. G. 2004. Plasma interaction of Io with its plasma torus. In: F. Bagenal, T. Dowling, and W. McKinnon (eds.), *Jupiter: The Planet, Satellites, and Magnetosphere*. Cambridge University Press, Cambridge, UK, pp. 537–560.

Simonelli, D. P., Dodd, C., and Veverka, J. 2001. Regolith variations on Io: Implications for bolometric albedos. *Journal of Geophys. Res.*, **106**, 33241–33252.

Spencer, J. R., Rathbun, J. A., Travis, L. D., Tamppari, L. K., Barnard, L., Martin, T. Z., and McEwen, A. S. 2000a. Io's thermal emission from the Galileo photopolarimeter–radiometer. *Science*, **288**, 1198–1201.

Spencer, J. R., Jessup, K. L., McGrath, M. A., Ballester, G. E., and Yelle, R. 2000b. Discovery of gaseous S_2 in Io's Pele plume. *Science*, **288**, 1208–1210.

Turtle, E. P., Jaeger, W. L., Keszthelyi, L. P., McEwen, A. S., Milazzo, M., Moore, J., Phillips, C. B., Radebaugh, J., Simonelli, D. P., Chuang, F., *et al.* 2001. Mountains on Io: High-resolution Galileo observations, initial interpretations, and formation models. *Journal of Geophys. Res.*, **106**, 33175–33199.

Turtle, E. P., Keszthelyi, L., McEwen, A. S., Radebaugh, J., Milazzo, M., Simonelli, D. P., Geissler, P., Williams, D. A., Perry, J., Jaeger, W. L., *et al.* 2004. The final Galileo SSI observations of Io: Orbits G28–I33. *Icarus*, **169**, 3–28.

Vasyliunas, V. M., Frank, L. A., Ackerson, K. L., and Paterson, W. R. 1997. Geometry of the plasma sheet in the midnight-to-dawn sector of the Jovian magnetosphere: plasma observations with the Galileo spacecraft. In: *Geophysical Research Letters* (vol. 24). American Geophysical Union, Washington, D.C., pp. 869–872.

Williams, D. A., Davies, A. G., Keszthelyi, L. P., and Greeley, R. 2001. The summer 1997 eruption at Pillan on Io: Implications for ultrabasic lava flow emplacement. *Journal of Geophys. Res.*, **106**, 33105–33119.

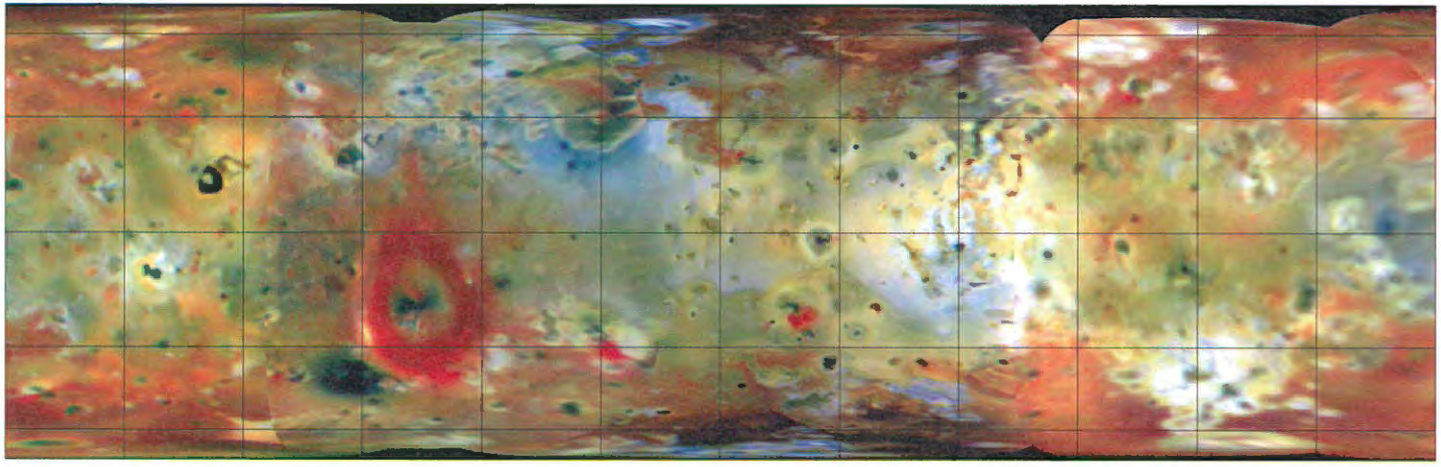

Figure 3.2. Color mosaic of images taken during the 1st and 2nd orbits during the *Galileo* nominal mission. A grid was overlain with 30° by 30° spacing. Numerous changes were observed between *Voyager* and *Galileo* but the overall pattern of volcanic centers and overall color variation was still recognizable, indicating that surface changes were limited to the area around volcanic centers that repeatedly erupted (NASA press release image PIA00585).

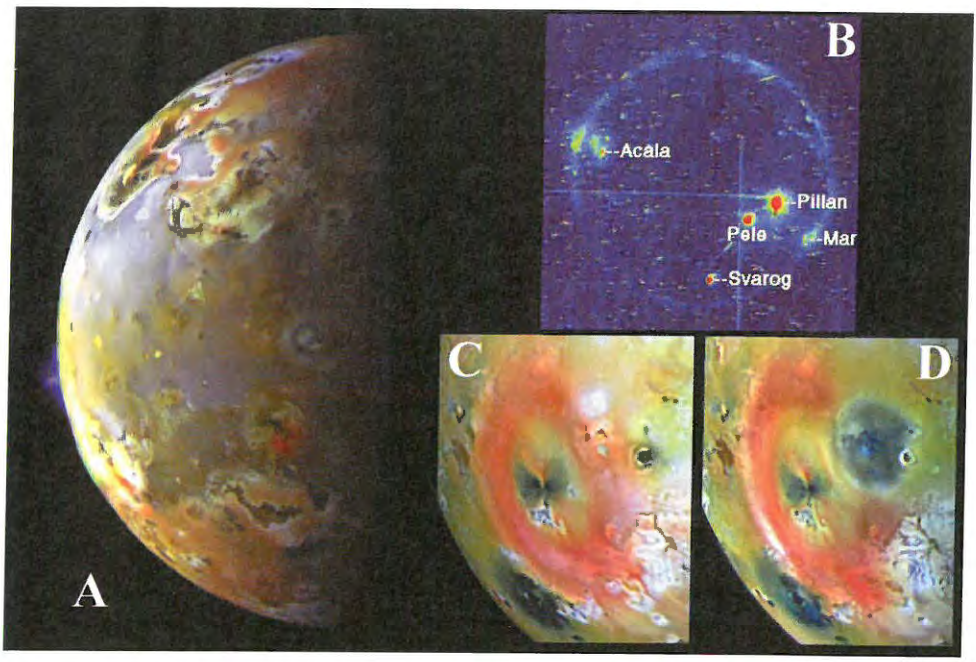

Figure 3.3. Several views of the summer 1997 eruption of Pillan Patera. North is up in all panels. (A) Shows a moderate phase angle image taken during orbit 9 (C9), showing the plume over Pillan at the limb. This observation was taken from a distance of 600,000 km and has a resolution of 6 km per pixel. (B) Shows an eclipse observations from orbit 9 showing the intensity of the Pillan eruption at the time. That observation was taken from a distance of 1.46 million kilometers and has a resolution of 14.6 km per pixel. The image has been color-coded for intensity, with red being the most intense signal. Both (C) and (D) show the aftermath of the Pillan eruption, with a new dark deposit surrounding Pillan Patera in (D). Pele and the ring that surrounds it can be seen to the south-east of Pillan. (C) Was taken during orbit 7 in April 1997 from a distance of 563,000 km, and has a resolution of 5.63 km per pixel. (D) was taken during orbit 9 in September 1997 from a distance of 506,000 km, and has a resolution of 5.06 km per pixel (NASA press release images PIA00703, PIA01635, PIA00744).

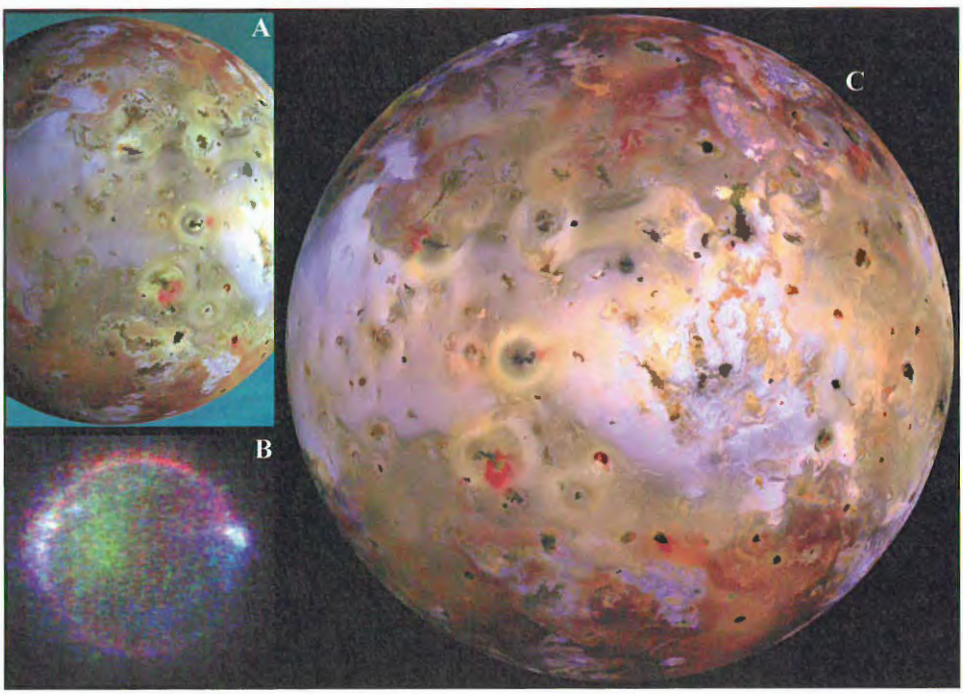

Figure 3.4. Imaging highlights from the Europa and perijove reduction phases of the GEM. (A) A mosaic of two, three-color frames showing the anti-Jovian hemisphere, taken during orbit 14 from a distance of 290,000 km with a resolution of 2.9 km per pixel. (B) A three-color observation of Io during eclipse. The faint red glows represent emissions from atomic oxygen and green glows from atomic sodium, while the bright blue emissions near the equator are likely due to electron impacts on SO_2. Image (B) was taken during orbit 15 from a distance of 1.4 million km and has a resolution of 14 km per pixel. (C) A large, three-color, 16-frame mosaic taken during orbit 21. This mosaic represents the highest resolution view of Io by *Galileo* prior to the Io-targeted encounters later in the mission. The images in this mosaic were taken from a distance of 130,000 km and have a resolution of 1.3 km per pixel (NASA press release images PIA01604, PIA01637, PIA02309).

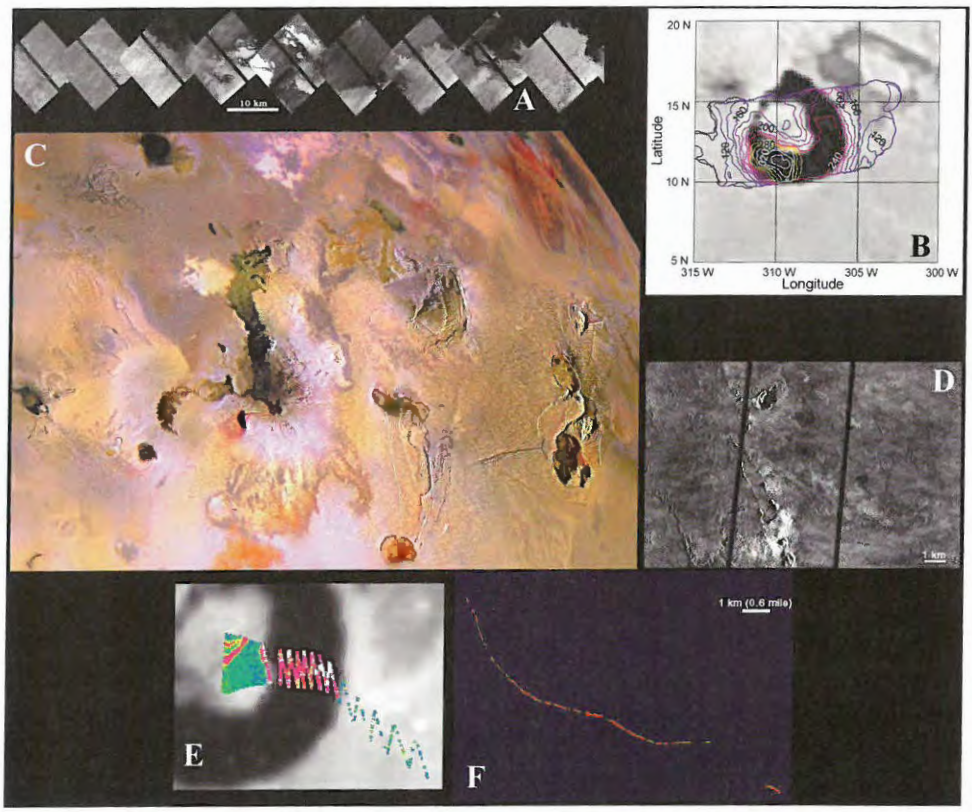

Figure 3.5. Highlights from the I24 fly-by of Io. (A) The ZAMAMA01 observation from I24. (B) Temperature map of Loki Patera taken by the PPR instrument. (C) AMSKIGI01 observation merged with color from orbit 21. (D) Portion of the PILLAN01 observation showing pits and rafted plates within the Pillan flow field. (E) NIMS observation of Loki Patera from shortly before the closest approach. (F) PELE_01 observation with a string of hot spots marking the margin of the Pele lava lake (NASA press release images PIA02537, PIA02524, PIA02526, PIA02536, PIA02514, PIA02511).

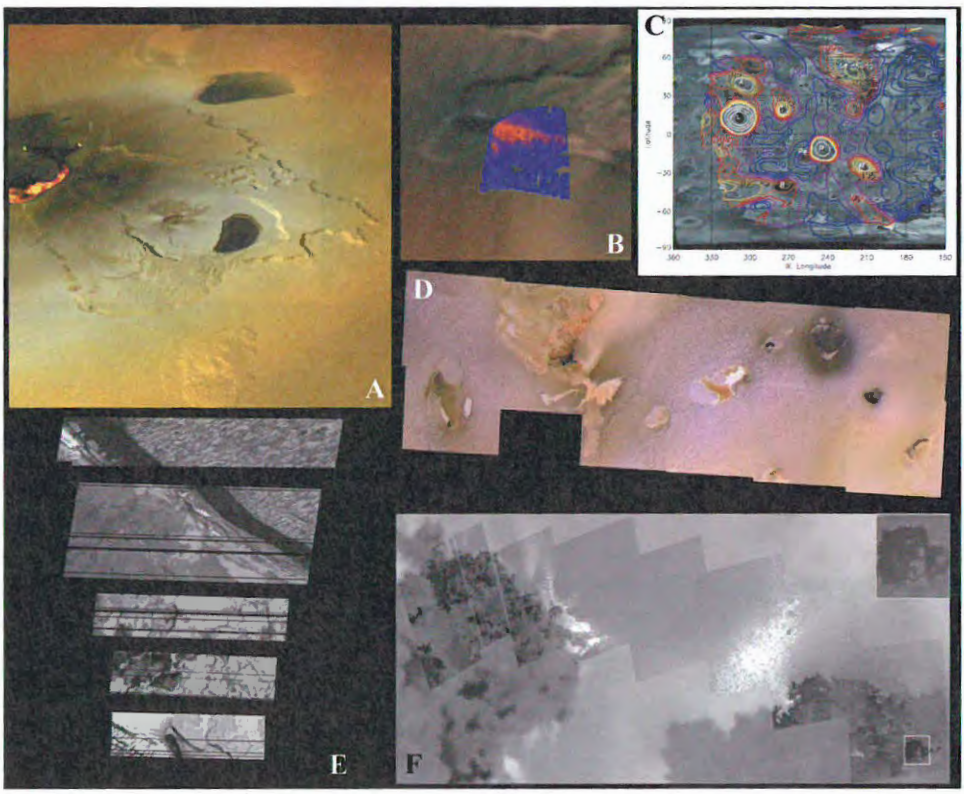

Figure 3.7. Highlights from the I27 fly-by. (A) False-color view of Tvashtar Paterae from the TVASHT01 observation. (B) NIMS observation of the Pele caldera overlain on a false-color image from *Voyager 1*. (C) Map of night-time temperatures of Io's trailing hemisphere taken by the PPR instrument. (D) CAMAXT01 observation merged with color from orbit 21. (E) Partial frames from the CHAAC01 observation. Frames showing the north-east margin of Chaac Patera are see at the top while frames showing the floor and the south-west margin are seen at the bottom. (F) PROMTH01 observation. A dark flow with two spots of incandescent lava is highlighted to the right (NASA press release images PIA02550, PIA02560, PIA02548, PIA02566, PIA02551, PIA02564).

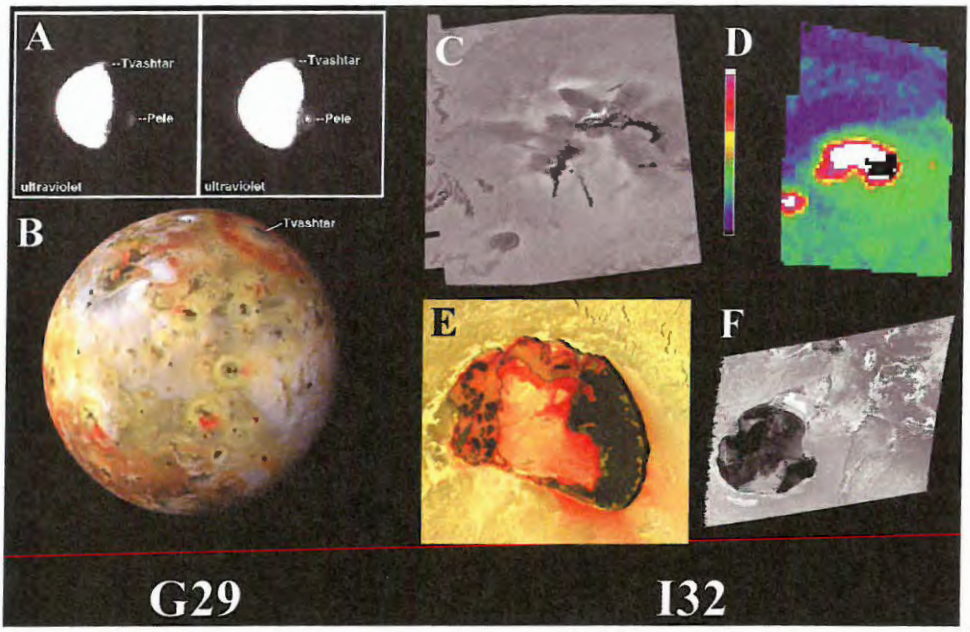

Figure 3.8. Highlights from orbit 29 and I32. Both (A) and (B) highlight a new eruption at Tvashtar observed during late 2000. The two figures in (A), enhanced images from the *Cassini* spacecraft, show a 385 km tall plume over Tvashtar as well as the plume over Pele. As seen in (B) from *Galileo*, both plumes have formed large red ring deposits. Panels (C–F) show highlights from the I32 fly-by. Both (C) and (D) show a new eruption at Thor, first seen by NIMS during I31 and in distant observations from the same orbit. Image (C) is taken from the TERMIN02 observation while (D) is a 13–16 km per pixel observation from NIMS. (E) Color observation of Tupan Patera, from the observation TUPAN_01. (F) Frame from the observation GSHBAR01, revealing fresh lava flows on its surface.

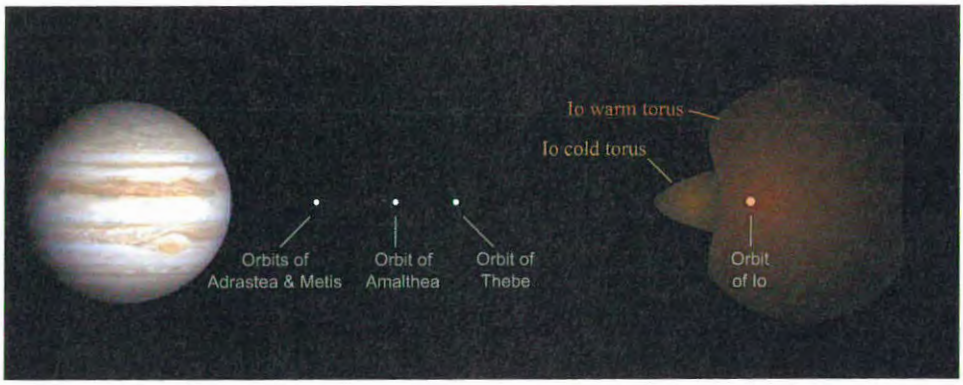

Figure 3.9. This figure illustrates both the warm and cold torus of Io. The *Galileo* spacecraft was able to sample the cold torus on the 34th orbit of Jupiter just before its final trajectory loop around Jupiter on J35. Courtesy Windows to the Universe *www.windows.ucar.edu* A34 Interactive Graphic.

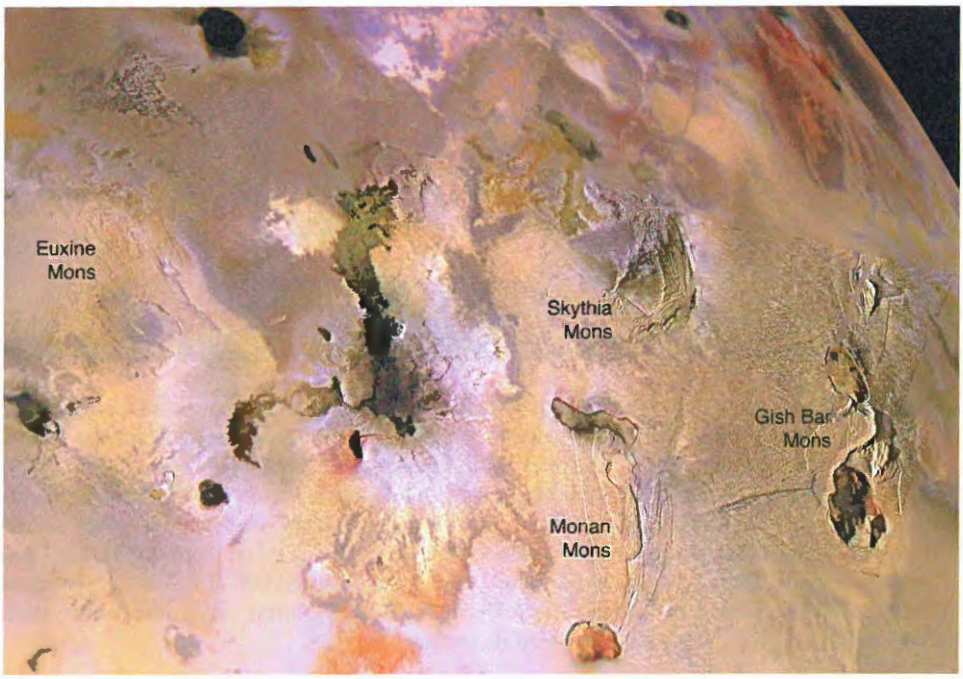

Figure 6.1. This moderate-resolution, ~500 m per pixel, regional mosaic combined with lower resolution, 1.3 km per pixel, color images acquired by *Galileo* includes several examples of Ionian mountains and volcanic centers. The mountains are isolated from each other, but a high fraction of those in this region are associated with paterae. The illumination, which is from the left, accentuates the topography and surface textures. This effect is strongest on the eastern side where the solar incidence angle is 21–28° and weakens toward the west where the Sun is higher, solar incidence angle ~37–45°: compare the visibility of ~10 km high Gish Bar Mons, between Gish Bar Patera to the south and Estan Patera to the north; ~6 km high Monan Mons, between Monan Patera to the north and Ah Peku Patera to the south; and ~7 km high Euxine Mons.